Rheology of growing axons

Hadrien Oliveri [1], Rijk de Rooij [2], Ellen Kuhl [2] and Alain Goriely [1,*]
[1]*Mathematical Institute, University of Oxford, Oxford OX2 6GG, United Kingdom*
[2]*Department of Mechanical Engineering, Stanford University, Stanford, California 94305, USA*

(Received 28 March 2022; accepted 11 July 2022; published 12 August 2022)

The growth of axons is a key process in neural system development, which relies upon a subtle balance between external mechanical forces and remodeling of cellular constituents. A key problem in the biophysics of axons is therefore to understand the overall response of the axon under stretch, which is often modeled phenomenologically using morphoelastic or viscoelastic models. Here, we develop a microscopic mixture model of growth and remodeling based on protein turnover and damage to obtain the macroscopic rheology of axonal shafts. First, we provide an estimate for the instantaneous elastic response of axons. Second, we predict that under moderate traction velocities, the axonal core behaves like a viscoelastic Maxwell material whose rheological parameters can be expressed in terms of the microscopic properties. Third, for larger velocities, we show that failure takes place due to extensive damage.

DOI: 10.1103/PhysRevResearch.4.033125

I. INTRODUCTION

Neurological functions rely on the exchange of electrochemical signals between neurons via slender cellular processes called *axons* [1,2]. During early neurodevelopment, neuronal cell bodies project axons that extend through the extracellular environment to connect with other target cells [3,4]. Then, once connected via synapses, axons passively elongate to accommodate the growth of the embedding medium [5,6]. During this so-called *stretch growth* phase, growth kinematics is fully dictated by the animal's body expansion. In normal growth conditions, axonal elongation is supported by the addition of cell material, allowing the axon to sustain stretch and maintain structural homeostasis [7–10]. However, upon faster stretch, this mechanism may fail, triggering a cascade of pathophysiological responses that, ultimately, converge to irreversible axonal damage [11–16]. A question is then: How does the axon respond mechanically and structurally to various stretch rates?

Typically, macroscopic—viscoelastic or morphoelastic—models are used to capture the mechanical response of growing axons [7,12,17–25]. These simple models can be easily treated mathematically and compared with experiments [26]; however, they are phenomenological and are not explicitly linked to the microstructural changes occurring in the axoplasm during growth. Alternatively, detailed computational models have been proposed to study the role of individual proteins within the cytoplasm [13,27–39]; typically, a core of parallel *microtubules* cross linked by microtubule-associated *tau proteins* [Fig. 1(a)]. This approach captures the subtle mechanical interactions between key molecular actors and the emergent rheology; however, it is relatively complex and does not produce macroscopic models.

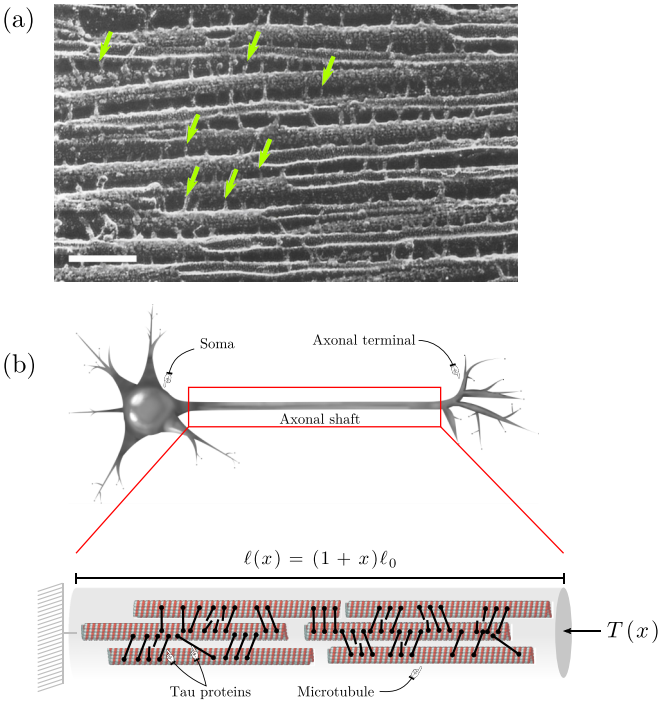

FIG. 1. (a) Electron microscopy image of porcine brain microtubules cross linked with tau proteins shown by arrows. Scale bar = 100 nm. Adapted from [41] with permission from Rockefeller University Press. (b) Neuronal axon subject to an imposed strain $x(t)$. The cytoskeleton is modeled as a well-mixed phase composed of microtubules and tau proteins that may attach, and then detach depending on their individual tension $F(t)$. The individual protein tension results at a global scale in a macroscopic tension $T(t)$.

*goriely@maths.ox.ac.uk

Here, we start with the key structural constituents of an axon, i.e., microtubules and tau proteins, to derive a macroscopic, homogenized rheological model of axonal stretch growth. We show that under moderate pulling velocities, the axon behaves like a viscoelastic Maxwell material [24,40], and the model captures the stress-strain response predicted by a previous computational approach [32]. Conversely, for higher stretch rates, remodeling is not fast enough and cross linking becomes deficient.

II. MODEL

Our model contains two main structural elements: the microtubules and the cross-linking tau proteins. We consider a homogeneous cylindrical axon of initial length ℓ_0 containing M_0 parallel microtubules of length a cross linked by N_0 tau proteins [Fig. 1(b)]. We consider a steady traction scenario in which the axon is towed at a constant stretch rate ξ, so that its current length is given by $\ell(t) = \ell_0(1 + \xi t)$, where t denotes the time elapsed since the beginning of traction. Assuming that the cytoplasmic constituents form a well-mixed phase, and neglecting inertial effects, the strain $x = \xi t$ is uniform along the axon (as seen in the kymograph shown in [31]). As the axon elongates, microtubules slide with respect to one another, which stretches the cross links and promotes their detachment. Following [13,32,36,42], we assume that the tau dissociation kinetics follows a Bell-type model [43] in which a population of $N(t)$ cross links subject to a force $F(t)$ detaches according to

$$\frac{dN}{dt} = -k_{\text{off}} e^{F/F_0} N, \tag{1}$$

where k_{off} is the load-free dissociation rate, and F_0 is a characteristic bond force. We model each protein as a linear spring with constant κ and deformation d, which provides the force $F = \kappa d$. Since microtubules are orders of magnitude stiffer than tau proteins [44–47], we further postulate that they remain rigid.

A difficulty is that cross links attach to different microtubules, which may slide with respect to one another with different velocities (Appendix A). In addition, in a remodeling axon, different cross links are formed at different times. These specificities require modeling the axoplasm as a mixture of cross links with different mechanical states. Assuming a protein is attached at strain x', its deformation at $x \geqslant x'$ is modeled as

$$d(x, x') = d_0 \frac{x - x'}{1 + x'}, \tag{2}$$

where $d_0 = a/\sqrt{6}$ is obtained by a strain-energy-based homogenization argument (Appendix A). The total population of cross links at strain x is then given by the mixture [42]

$$N(x) = N_0 \mathcal{G}(x, 0) + \int_0^x S(x') \mathcal{G}(x, x')\, dx', \tag{3}$$

where S is the binding rate (per unit strain x), detailed later; and where the kernel

$$\mathcal{G}(x, x') = \exp\left\{ \frac{q}{\nu}(1 + x') \left[1 - \exp\left(\frac{1}{q} \frac{x - x'}{1 + x'} \right) \right] \right\} \tag{4}$$

is obtained by solving Eq. (1) in terms of x for some initial strain x' (Appendix B). The dimensionless parameters $q := F_0/\kappa d_0$ and $\nu := \xi/k_{\text{off}}$ characterize the bond dissociation force and the pulling speed, respectively. The first term in Eq. (3) represents the decaying population of initial cross links. The second term accounts for the cross links formed at all strains $x' \in [0, x]$ during traction, and disconnecting progressively as x increases. To simplify notations, we introduce a mixture operator $\mathfrak{M}$ that can be applied to any extensive property $\mathcal{P}(x, x')$ of the cross links as

$$\mathfrak{M}[\mathcal{P}](x) = N_0 \mathcal{P}(x, 0) \mathcal{G}(x, 0) + \int_0^x S(x') \mathcal{P}(x, x') \mathcal{G}(x, x')\, dx', \tag{5}$$

so that, e.g., Eq. (3) becomes $N = \mathfrak{M}[1]$.

The mechanical response of the axon under applied stretch can be deduced from the individual cross-link strain energies,

$$\mathcal{W}(x, x') = \tfrac{1}{2} \kappa d(x, x')^2, \tag{6}$$

from which we obtain the total energy of the system, $W = \mathfrak{M}[\mathcal{W}]$. By the principle of virtual work for an axon under tension $T(x)$, we have $T \delta \ell = T \ell_0 \delta x = \delta W$, where the virtual work δW is the sum of all virtual works due to the cross links,

$$\delta W = \mathfrak{M}[\delta \mathcal{W}] = \mathfrak{M}\left[\frac{\partial \mathcal{W}}{\partial x} \right] \delta x. \tag{7}$$

Thus,

$$T = \mathfrak{M}\left[\frac{\partial \mathcal{W}}{\partial x} \right], \quad \frac{\partial \mathcal{W}}{\partial x}(x, x') = \frac{\kappa d_0^2}{\ell_0} \frac{x - x'}{(1 + x')^2}. \tag{8}$$

The state of the mixture depends on the attachment of new cross links with rate $S(x)$ from either new free tau proteins supplied by the cell or detached proteins that can form new connections [32,37]. Assuming a pool of $\widetilde{N}$ available proteins with uniform concentration $\widetilde{N}/\ell$ along the axon (nonlimiting transport), a simple model for S is $S dx = k_{\text{on}} \widetilde{N} dt$, where k_{on} is an effective on-rate constant [48]. The number of free proteins then follows

$$\frac{d\widetilde{N}}{dt} = I + \beta k_{\text{off}} R - k_{\text{on}} \widetilde{N}, \tag{9}$$

where I is a source term, $k_{\text{off}} R$ is the number of cross links disconnected per unit time [Eqs. (1) and (2)],

$$R = \mathfrak{M}[\mathcal{R}], \quad \mathcal{R}(x, x') := \exp\left(\frac{1}{q} \frac{x - x'}{1 + x'} \right), \tag{10}$$

and β is the probability of a protein being available for reattachment after disconnection. We hypothesize that the cell aims to maintain a target lineal density $\widetilde{N}_0/\ell_0$ (i.e., number of free proteins per unit longitudinal length), and therefore we posit $I = I_0[\widetilde{N}_0(1 + x) - \widetilde{N}]$, with $I_0 \geqslant 0$ a constant.

The case $\beta > 0$ is solved numerically (Appendix D). Figure 2(a) shows the effect of reattachment on the primary cross-link population—the population initially present in the axon—in the absence of synthesis ($I_0 = 0$). As expected, for $\beta < 1$, the cross links are eliminated faster than exponentially; larger β promotes slower elimination, as cross links can operate longer. For $\beta = 1$, however, the cross links disconnect and

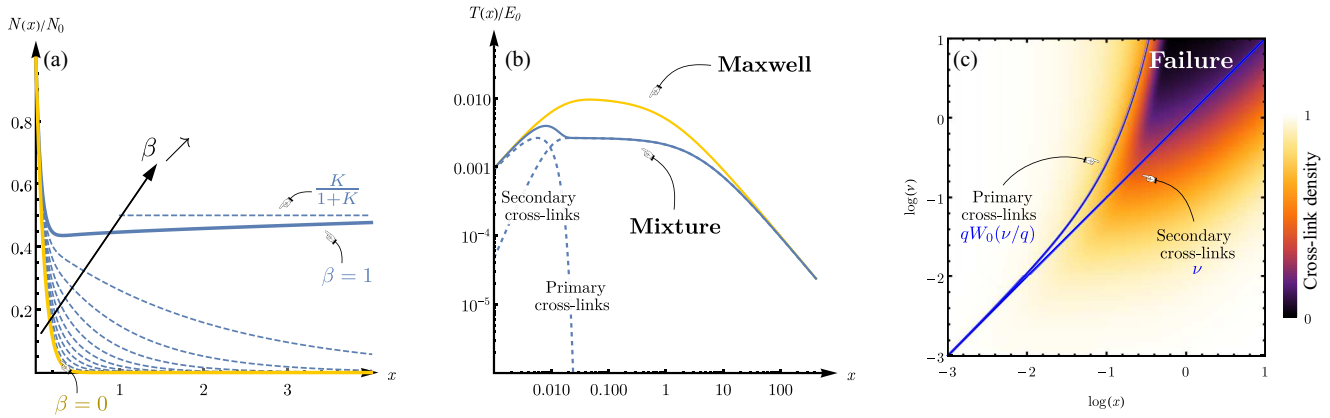

FIG. 2. (a) Effect of protein reattachment β for a initial population of cross links [Eqs. (9) and (10)] simulated numerically for different values of β, and with $I_0 = 0$ (no synthesis), $k_{\text{off}} = 0.1$, $K = 1$, $q = 1$, and $\nu = 0.1$. Blue and yellow lines show, respectively, the two extreme cases $\beta = 1$ (full reintroduction) and $\beta = 0$ (no reintroduction). Blue dashed lines show intermediate cases with $0 < \beta < 1$. (b) Log-log plot of the normalized tension T/E_0 vs strain x ($q = 0.1$, $\nu = 0.01$). Yellow and blue solid lines, respectively, show the Maxwell model Eq. (12) and the mixture model. Blue dashed lines show the contributions of the initial and new cross links. (c) Density $N(x)/\ell(x)$ (normalized by N_0/ℓ_0) vs strain x and parameter ν (logarithmic scale, $q = 0.1$). Solid lines show the characteristic strain scales of the initial (x_{I}, top) and newly formed (x_{II}, bottom) populations of cross links.

reattach endlessly and $N \to N_0 K/(1+K)$, with $K := k_{\text{on}}/k_{\text{off}}$ the binding constant.

We henceforth consider the ideal case where detached cross links do not reattach, $\beta \approx 0$. Assuming $I_0 \gg k_{\text{on}}$, a solution to Eq. (9) is $\widetilde{N}(x) \approx \widetilde{N}_0(1+x)$ (constant lineal density $\widetilde{N}_0/\ell_0$), giving

$$S(x) \approx \frac{K\widetilde{N}_0}{\nu}(1+x). \tag{11}$$

Assuming chemical equilibrium initially, we have $N_0 = K\widetilde{N}_0$, and the dynamics is fully governed by q and ν.

Initially, for small strain x, the response under tension due to the primary cross links is Hookean, namely, $T(x) \approx E_0 x$ with stiffness modulus $E_0 := N_0 \kappa d_0^2/\ell_0$ [Fig. 2(b)]. Tension then peaks when $x = qW_0(\nu/q)$ (where W_0 is the Lambert function). This peak strain provides a typical *strain-scale* x_{I} for the primary cross-links persistence [Fig. 2(c)]. Past the peak, primary cross-links tension quickly vanishes as the cross links disconnect faster than exponentially [Eqs. (3) and (4)].

The secondary newly formed cross links initially contribute only to $\sim E_0 x^2/2\nu$ to the tension; they do not participate in the linear elastic response, as they are not yet connected and under tension. For large strains, however, the total tension is only due to the new cross links and, as the local strain rate decreases [Eq. (2)], the tension vanishes slowly as $T(x) \sim E_0\nu/x$ [Fig. 2(b), Appendix C 1]. Simultaneously, the cross-link density reaches a homeostatic level $N_0 I_0/\ell_0(I_0 + k_{\text{on}}) \approx N_0/\ell_0$ with strain scale $x_{\text{II}} = \nu$ [Fig. 2(c)].

Depending on whether stretch is applied in a physiological, experimental, or traumatic context, the parameter ν may be either very small or very large. For rapid stretch, $\nu \gg 1$, we see that $x_{\text{I}} \ll x_{\text{II}}$: The primary cross links disconnect before the secondary cross-link density reaches a sufficient level to maintain integrity, and the core ruptures [Figs. 2(a) and 2(b)]. Note that, in this regime where density decreases, the well-mixedness assumption fails as random heterogeneities and inertial effects dominate, and the number of load paths along the axon also decreases [13,31]. Conversely, for slow towing, $\nu \ll 1$, we have $x_{\text{I}} \approx x_{\text{II}}$: New cross links replace the disconnected ones and rescue the axon core. The critical tau deficit, at which the axon is most vulnerable, is given by $D = \max_x\{1 - N(x)/N_0(1+x)\}$ and, for ν small, we have $D \approx (1+q^{-1})\nu$. Remarkably, in this regime, the model reduces to a viscoelastic Maxwell-like material, with extensional stiffness E_0 and effective viscosity $\eta_0 := E_0/k_{\text{off}}$ (Appendix C 2), namely,

$$\frac{1}{E_0}\frac{dT}{dt} + \frac{T(t)}{\eta_0} = \frac{1}{\ell(t)}\frac{d\ell}{dt}. \tag{12}$$

Note that this is not the standard form for a Maxwell material, which has nonzero tension at infinity [24,40]. Here, our Maxwell-like material has the property that tension goes to zero at infinity. This is due to the fact that growth takes place along the entire axon shaft, with a local stretch rate that decreases as $\sim 1/\ell$.

For an axon of diameter $\approx$0.5 μm [32], with $N_0/\ell_0 \approx 100\ \mu\text{m}^{-1}$ [32], $\kappa = 0.01$–0.1 pN nm^{-1} [37], and $a = 10\ \mu$m [32], we estimate a Young's modulus (E_0 normalized by cross section) of the order of $\sim$10–100 kPa, which compares with the value reported by [19]. Combining this estimate with the measured axon viscosity $\eta_0 = 10^6$–10^7 Pa s [21], we estimate $k_{\text{off}} \sim 10^{-3}$–$10^{-1}$ s^{-1}; however, considering reattachment should, in principle, yield larger estimates for k_{off}. The force F_0 can be expressed as $F_0 = k_{\text{B}}T/\chi$, with χ the typical bond separation distance, and $k_{\text{B}}T \approx 4$ pN nm. Then, estimating $\chi \approx 1$ nm, we obtain $F_0 \sim$ 1–10 pN [31] and $q \sim 10^{-3}$–10^{-1}.

III. DISCRETE SIMULATIONS

Last, we compare our homogenized model against the discrete finite-element model detailed in [32]. We consider a bundle of $M_0 \approx 50$ randomly placed parallel microtubules, connected via $N_0 \approx 5000$ dynamically breaking cross links, and we test three different pulling velocities, $\nu = 0.01$, 0.04, and 0.1. For simplicity, here we ignore remodeling ($\beta = 0$, $S = 0$) (see [32] and Appendix E for details). We see in

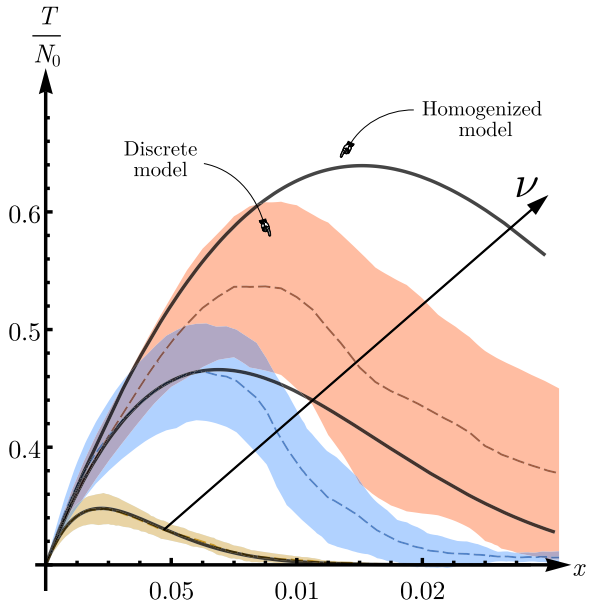

FIG. 3. Comparison of our homogenized model with the discrete finite-element model of [32]. Tension-strain curves T/N_0 vs x, for $\nu = 0.01$, 0.04, 0.07, and 0.1. Solid lines correspond to the homogenized model. Colored streaks show the mean and standard deviation for 14 simulations of the discrete model for each value of ν.

Fig. 3 that for moderate velocities, the homogenized model faithfully reproduces the stress-strain curves from the discrete simulations; in particular, note the excellent approximation in the initial Hookean regime ($x \ll 1$), obtained with no fitting parameter. For higher stretch rates, however, as expected, localized heterogeneities in the discrete model dominate the yielding process, which results in the homogenized model overestimating the tension.

IV. DISCUSSION

Healthy growth relies on a subtle balance between mechanics, transport, and synthesis of proteins, and cell remodeling [24]. Using mixture theory combined with a Bell-type model for tau disconnection [13,32,36,42,43], we propose a mechanistic macroscopic model for the mechanical response of stretched axons. In contrast to more realistic, but mathematically intractable, computational models [13,27–37], this coarse-grained approach establishes a direct mathematical link between cellular parameters and the emergent rheology of axons. First, we derived an expression of the axon's extensional stiffness: $E_0 \approx N_0 \kappa a^2/6\ell_0$. Denoting ρ and $\tilde{\rho}$ the lineal densities of cross linking and microtubules, respectively, we obtain the scaling law $E_0 \propto \rho\tilde{\rho}^2 a^4$, which explicitly relates the microstructural geometry to the overall elastic response [39]. Second, we showed that rate-dependent effects emerge from the energy-dissipating disconnection of linearly elastic cross links embedded in a dynamically evolving mixture, as also shown in [31]. For small strain rates, we proved that the system behaves like a Maxwell viscoelastic material, with extensional stiffness E_0 and viscosity $\eta_0 = E_0/k_{\text{off}}$. This prediction recovers the observed fluidlike behavior of axons [12,18,19,21,22] and corroborates previous computational study [31]. For higher strain rates, however, a critical regime appears where the axon fails to maintain a sufficient level of cross linking due to insufficient remodeling, with a critical tau deficit attained around the characteristic strain $x_{\text{I}} = qW_0(\nu/q) \approx \nu$. Note, however, that subtler rate-dependent effects could potentially emerge from more sophisticated viscoelastic models of individual tau and microtubules [36,37], or by taking into account the actomyosin sheath of the axon that generates active forces [22,33,49]. Neuronal injury involves many other mechanisms such as microtubule breakage and collapse [15,16,36,37,50]. Here, we have ignored these effects of extreme axonal mechanics to focus our attention on the evolution of microtubule cross linking during slow growth. By definition, growth is limited by mass uptake [24], and, in singularly large and fast growing cells such as neurons, an important question is what mechanisms regulate material availability [5,9]. Here, we found that a linear coupling between axonal length ℓ and protein synthesis rate I was adequate to maintain sufficient material supply. Biologically, this modeling assumption implies a hypothetical level of regulation to control the production of new proteins, e.g., a length detection [10,51], or a direct sensing of the free cross-links concentration.

Axonal growth is the central component of neurodevelopment. It obeys intricate rules with multiple interplays between mechanics, kinematics, biological feedback, remodeling, and protein supply. The detailed response of axons to stimuli and loads remains elusive, yet, based on universal microscopic principles related to attachment and detachment of cross links, their macroscopic response can be obtained and systematically compared with experiments by targeting specific microscopic properties. This type of approach opens the door to more refined multiscale theories of axonal growth.

ACKNOWLEDGMENTS

A.G. acknowledges support from the Engineering and Physical Sciences Research Council of Great Britain under research Grant No. EP/R020205/1. E.K. acknowledges support from the National Science Foundation under research Grant No. CMMI 1727268.

APPENDIX A: DETAILS OF THE MODEL

Here, we provide details on the assumptions underlying the mixture model previously developed. We consider the two main structural elements of the axon, i.e., rigid microtubules cross linked by stretchable tau proteins. Microtubules are long filamentlike polymers that, in the axon, are mostly aligned longitudinally and parallel to one another. We assume that they are fully aligned to the longitudinal axis of the axon and that they can only move by translation along that axis. Hence, our model is one dimensional and we are interested in the longitudinal mechanical response of the axon as a result of the interaction between microtubules and tau proteins [13,27–33,39].

1. Kinematics of tau protein deformation

Here, we study how a given cross link deforms when the whole axon undergoes a strain x. In a deformation of the

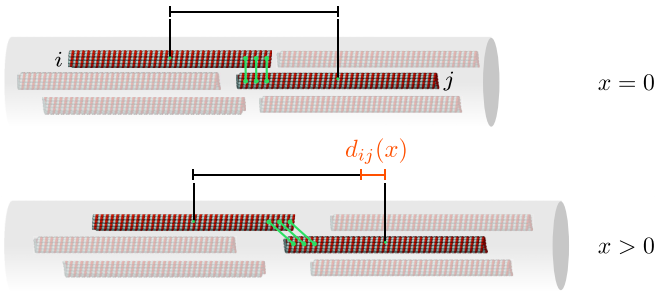

FIG. 4. Deformation of cross links connecting two microtubules i and j. The rate of deformation depends on the distance between the two microtubules, whose respective centers of mass undergo affine displacement.

axon, microtubules slide with respect to one another, which in turn stretches the connecting cross links. For simplicity, we neglect the growth and shrinkage of microtubules that might result in net migration of the microtubules along the axon. Thus, we assume that all microtubules have identical and constant length a. Considering that microtubule cross links are homogeneously distributed along the axon, we also assume that each microtubule's center of mass (midpoint) moves according to an affine transformation, i.e., its center of mass is passively advected with the embedding medium, so that the longitudinal motions of microtubules are imposed geometrically. Namely, if p is the longitudinal position of a microtubule's midpoint, then, for any strains x and x' of the axon, we have

$$\frac{p(x)}{1+x} = \frac{p(x')}{1+x'}. \tag{A1}$$

Now, consider a cross link created at strain x' and connected to two different microtubules i and j with respective positions p_i and p_j. Neglecting the nonlinear effects due to the small lateral distance between the two microtubules, the gradient of tau displacement with respect to the global strain x is given by

$$\frac{\partial d_{ij}}{\partial x} = \left|\frac{\partial p_j}{\partial x} - \frac{\partial p_i}{\partial x}\right| = \frac{|p_j(x') - p_i(x')|}{1+x'}, \tag{A2}$$

which can be integrated to obtain

$$d_{ij}(x, x') = |p_j(x') - p_i(x')| \times \frac{x - x'}{1+x'}. \tag{A3}$$

Hence, different cross links attached at the same strain x' will undergo different deformations, depending on the relative positions of their microtubules (Fig. 4).

2. Elastic response

Here we focus on the initial Hookean elastic response, with $x' = 0$ and $x \ll 1$, and we assume that the cross links do not attach or dissociate. The total strain energy of the system can be obtained from Eq. (A3) by integrating the individual protein energies with spring constant κ,

$$\mathcal{W}_{ij}(x) = \tfrac{1}{2}\kappa d_{ij}(x,0)^2 = \tfrac{1}{2}\kappa(X_j - X_i)^2 x^2, \tag{A4}$$

over all possible initial longitudinal positions $X_i = p_i(0) \in [a/2, \ell_0 - a/2]$ of the M_0 microtubules, taken to be uniformly distributed along the axon:

$$W(x) = \left(\frac{M_0}{\ell_0 - a}\right)^2 \int_{a/2}^{\ell_0 - a/2}\int_{a/2}^{\ell_0 - a/2} \times n(X_i, X_j)\mathcal{W}_{ij}(x)\, dX_i\, dX_j. \tag{A5}$$

Here, $n(X_i, X_j)$ is the number of cross links connecting two overlapping microtubules located at positions X_i and X_j. We assume that $n(X_i, X_j)$ is proportional to the overlapping distance, i.e., $n(X_i, X_j) = \rho(a - |X_i - X_j|)_+$, where $(\cdot)_+$ is the ramp function and ρ is a lineal density of cross linking that is linked to N_0, the number of cross links, via

$$N_0 = \left(\frac{M_0}{\ell_0 - a}\right)^2 \int_{a/2}^{\ell_0 - a/2}\int_{a/2}^{\ell_0 - a/2} \times n(X_i, X_j)\, dX_i\, dX_j. \tag{A6}$$

From Eq. (A5), we also obtain the extensional stiffness,

$$E_0 = \frac{\kappa}{\ell_0}\left(\frac{M_0}{\ell_0 - a}\right)^2 \int_{a/2}^{\ell_0 - a/2}\int_{a/2}^{\ell_0 - a/2} \times n(X_i, X_j)(X_j - X_i)^2\, dX_i\, dX_j. \tag{A7}$$

Assuming $a \ll \ell_0$ (long initial axon), Eq. (A6) simplifies to

$$N_0 = \frac{\rho M_0^2(3a^2\ell_0 - 4a^3)}{3(\ell_0 - a)^2} \approx \frac{\rho M_0^2 a^2}{\ell_0}. \tag{A8}$$

Then we integrate Eqs. (A5) and (A7) using Eq. (A8), to obtain

$$W(x) \approx \tfrac{1}{12} N_0 \kappa a^2 x^2 \tag{A9}$$

and

$$E_0 \approx \frac{N_0 \kappa a^2}{6\ell_0}. \tag{A10}$$

3. Protein dissociation and model simplification

To model the dissociation of proteins, we need to track all pairs of microtubules as shown above. Using the kernel provided in Eq. (4), Eqs. (A5) and (A6) become

$$N(x) = \left(\frac{M_0}{\ell_0 - a}\right)^2 \int_{a/2}^{\ell_0 - a/2}\int_{a/2}^{\ell_0 - a/2} n(X_i, X_j) \exp\left\{\frac{F_0}{\kappa\nu|X_i - X_j|}\left[1 - \exp\left(\frac{\kappa x|X_i - X_j|}{F_0}\right)\right]\right\} dX_i\, dX_j \tag{A11}$$

and

$$W(x) = \left(\frac{M_0}{\ell_0 - a}\right)^2 \int_{a/2}^{\ell_0 - a/2}\int_{a/2}^{\ell_0 - a/2} n(X_i, X_j)\mathcal{W}_{ij}(x) \exp\left\{\frac{F_0}{\kappa\nu|X_i - X_j|}\left[1 - \exp\left(\frac{\kappa x|X_i - X_j|}{F_0}\right)\right]\right\} dX_i\, dX_j. \tag{A12}$$

Next, to take into account added proteins, we track all tau associations and microtubule additions occurring at strain $x' \leqslant x$ [Eq. (3)], which, ultimately, will result in a triple integration (over x, X_j, and X_i).

To make progress, we instead adopt a coarse-grained approach and we next posit a characteristic length scale d_0 and substitute all protein deformations in Eq. (A3) with a unique deformation,

$$d(x) \approx d_0 x, \tag{A13}$$

where d_0 is chosen so as to obtain the same strain energy given by Eq. (A9). The new energy can be easily computed [Eq. (6)] and we see that

$$d_0 = \frac{a}{\sqrt{6}}. \tag{A14}$$

Note that d_0 is much larger than the typical size of the individual tau proteins (i.e., ∼50 nm, while $a \approx 10$ μm; see [32]), which implies that tau proteins stretch individually much faster than the entire axon does.

We extend this approach to growing axons by assuming that the density of microtubules does not vary much during the growth process, i.e., $M(x) \approx M_0(1 + x)$, and we postulate that we can use Eqs. (A13) and (A14) to represent every internal state of the mixture during the elongation process:

$$d(x, x') = d_0 \frac{x - x'}{1 + x'}. \tag{A15}$$

Note that this approach is justified by the fact that d_0 is independent of ℓ_0, and thus Eq. (A14) applies, in principle, to axons of arbitrary size ℓ.

Figure 5 shows a comparison of the tension $T(x)$ and number of cross links $N(x)$ obtained from Eqs. (A11) and (A12), and from the model simplification [Eqs. (A13) and (A14)], respectively. We see that for relatively slow pulling speeds, the approximation is in good agreement with the more detailed integral model. Indeed, we note that the tension in the homogenized model (in the absence of cross-link addition, for simplicity) peaks when $x = x_\mathrm{I} = qW(\nu/q)$ and is given by

$$T_{\max} \approx \frac{N_0 d_0^2 \kappa \nu}{\ell_0 e} \tag{A16}$$

when $\nu \ll 1$. Conversely, for $\nu \ll 1$ and for $a \ll \ell_0$, the tension derived from Eq. (A12), evaluated at $x = x_\mathrm{I}$, can be simplified as

$$T(x_\mathrm{I}) \approx \frac{N_0 a^2 \kappa \nu}{6 \ell_0 e}. \tag{A17}$$

From Eq. (A14), we see immediately that $T(x_\mathrm{I}) \approx T_{\max}$. Thus, in the limit of short microtubules and slow towing, the two models are equivalent to leading order, which characterizes the convergence of our homogenization method.

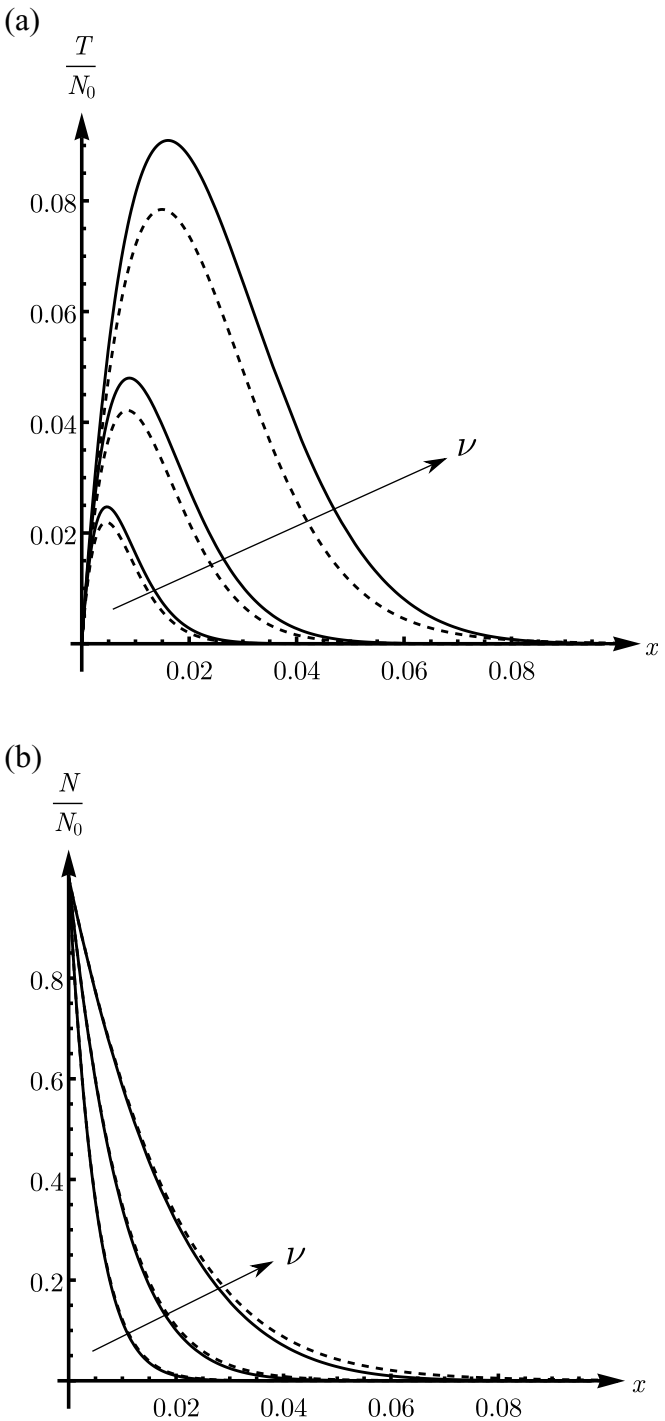

FIG. 5. (a) Axonal tension $T(x)/N_0$ and (b) number of cross links, $N(x)/N_0$, obtained by the integral model [Eqs. (A11) and (A12)] (dashed line), and by the single-length-scale model [Eqs. (A13) and (A14)] (solid line). Parameters given in Appendix E. We use $\nu = 0.005$, 0.01, and 0.02; and $S = 0$ (T expressed in pN).

APPENDIX B: DERIVATION OF THE KERNEL

Here we derive the kernel $\mathcal{G}$ given in Eq. (4). Combining Eqs. (A14) and (A15) with the approximate force $F(x, x') \approx \kappa d(x, x')$ applied at strain x to a cross link attached at strain x', we rewrite Eq. (1) as

$$\frac{dN}{dt} = -k_{\mathrm{off}} \exp\left(\frac{\kappa d_0}{F_0} \frac{x(t) - x'}{1 + x'}\right) N. \tag{B1}$$

Using the change of variable $x = \xi t$, and introducing $\nu = \xi/k_{\rm off}$ and $q = F_0/\kappa d_0$, we obtain

$$\frac{dN}{dx} = -\frac{1}{\nu}\exp\left(\frac{1}{q}\frac{x-x'}{1+x'}\right)N. \tag{B2}$$

The fundamental solution for this equation, obtained by direct integration between x' and x, is

$$\begin{aligned}\mathcal{G}(x,x') &= \exp\left[-\frac{1}{\nu}\int_{x'}^{x}\exp\left(\frac{1}{q}\frac{z-x'}{1+x'}\right)dz\right]\\ &= \exp\left\{\frac{q}{\nu}(1+x')\left[1-\exp\left(\frac{1}{q}\frac{x-x'}{1+x'}\right)\right]\right\}.\end{aligned} \tag{B3}$$

APPENDIX C: ASYMPTOTICS

We provide details of the asymptotic results given in the main text. We first study the case of small and large strains $x \ll 1$ and $x \gg 1$ (Appendix C 1), then we show that for slow stretch $\nu \ll 1$, the tension obtained with our mixture model is given asymptotically by the tension of a Maxwell material (Appendix C 2).

1. Cases $x \to 0$ and $x \to \infty$

The case $x \to 0$ is straightforward and can be obtained via a Taylor expansion of the various quantities of interest around $x = 0$. The case $x \to \infty$ can be studied using integration by part. By way of illustration, we derive the asymptotic behavior of the population $N(x)$ of attached cross links as $x \to \infty$. For clarity of notations, we can set $N_0 = 1$ and $E_0 = 1$, without loss of generality.

We first perform a change of variable $u = x'/x$ to fix the integration domain,

$$\begin{aligned}N(x) &\sim \int_0^x S(x')\mathcal{G}(x,x')\,dx'\\ &= x\int_0^1 S(ux)\mathcal{G}(x,ux)\,du\\ &= x\int_0^1 S(ux)e^{g(u)}\,du,\end{aligned} \tag{C1}$$

with

$$g(u) = \frac{q}{\nu}(1+ux)\left[1-\exp\left(\frac{x}{q}\frac{1-u}{1+xu}\right)\right]. \tag{C2}$$

We then extract the leading order through integration by part,

$$\begin{aligned}N(x) &\sim x\int_0^1 S(ux)e^{g(u)}\,du\\ &= x\int_0^1 \frac{S(ux)}{g'(u)}\,d(e^{g(u)})\\ &= \nu S(x) - \underbrace{x\int_0^1 e^{g(u)}\,d\left(\frac{S(ux)}{g'(u)}\right)}_{\text{h.o.t.}}\\ &\sim x.\end{aligned} \tag{C3}$$

Similarly, for the tension T, we integrate by parts twice to obtain

$$T(x) \sim \frac{\nu}{x}. \tag{C4}$$

2. Case $\nu \ll 1$: Maxwell model

We show that for slow growth $\nu \ll 1$ and fixed x, the model reduces asymptotically to the Maxwell model. For clarity of notation, here we note $\varepsilon = \nu$, the small parameter for the asymptotic analysis. In the case of a constant-speed traction that is considered, the Maxwell model, with extensional stiffness E_0 and viscosity $E_0/k_{\rm off}$, is defined via the tension $\widetilde{T}$ that obeys Eq. (12),

$$\widetilde{T}'(x) + \frac{1}{\varepsilon}\widetilde{T}(x) = \frac{1}{1+x}, \quad \widetilde{T}(0) = 0, \tag{C5}$$

where $(\cdot)'$ denotes the derivative with respect to x. The solution to Eq. (C5) is

$$\widetilde{T}(x) = \exp\left(-\frac{1+x}{\varepsilon}\right)\left[\mathrm{Ei}\left(\frac{1+x}{\varepsilon}\right) - \mathrm{Ei}\left(\frac{1}{\varepsilon}\right)\right], \tag{C6}$$

where Ei is the exponential integral function. For small ε, the solution can be expanded to obtain

$$\widetilde{T}(x) = \frac{\varepsilon}{1+x} - \varepsilon e^{-x/\varepsilon} + \mathcal{O}(\varepsilon^2). \tag{C7}$$

Next, we address the asymptotic behavior of the mixture model for $\varepsilon \ll 1$. In this case, the tension is given in terms of the integral,

$$\mathcal{I}(x) = \int_0^x \frac{x-x'}{1+x'}\mathcal{G}(x,x')\,dx', \tag{C8}$$

such that

$$T(x) = x\mathcal{G}(x,0) + \frac{1}{\varepsilon}\mathcal{I}(x). \tag{C9}$$

This integral is of the form

$$\mathcal{I}(x) = \int_0^x f(x')e^{\lambda g(x')}\,dx', \tag{C10}$$

with $\lambda = \varepsilon^{-1} \gg 1$; and with $f(x') = (x-x')/(1+x')$ and $g(x') = q(1+x')(1-e^{f(x')/q})$. The argument in the exponential is maximal for $x' = x$, thus we adapt Laplace's method of integration by expanding $g(x')$ and $f(x')$ to first order around $x' = x$, noting that $f(x) = g(x) = 0$:

$$\begin{aligned}\mathcal{I}(x) &\approx -f'(x)\int_0^x (x-x')\exp\left[-\lambda g'(x)(x-x')\right]dx'\\ &= \frac{1}{1+x}\int_0^x (x-x')e^{-\lambda(x-x')}\,dx'\\ &= \frac{1-(1+\lambda x)e^{-\lambda x}}{\lambda^2(1+x)}\\ &= \frac{\varepsilon^2 - \varepsilon(\varepsilon+x)e^{-x/\varepsilon}}{1+x}.\end{aligned} \tag{C11}$$

From Eqs. (C9) and (C11), we obtain

$$\begin{aligned}T(x) = \frac{\varepsilon}{1+x} - \frac{x+\varepsilon}{1+x}e^{-x/\varepsilon}\\ + x\exp\left[\frac{q}{\varepsilon}(1-e^{x/q})\right] + \mathcal{O}(\varepsilon^2),\end{aligned} \tag{C12}$$

which can be put under the form $T(x) = \widetilde{T}(x)(1+\delta(x) + \mathcal{O}(\varepsilon))$, with

$$\delta(x) = -\frac{x\left((x+1)\exp\left(\frac{q+x}{\varepsilon} - \frac{q}{\varepsilon}e^{x/q}\right) + \varepsilon - 1\right)}{\varepsilon(e^{x/\varepsilon} - x - 1)}. \tag{C13}$$

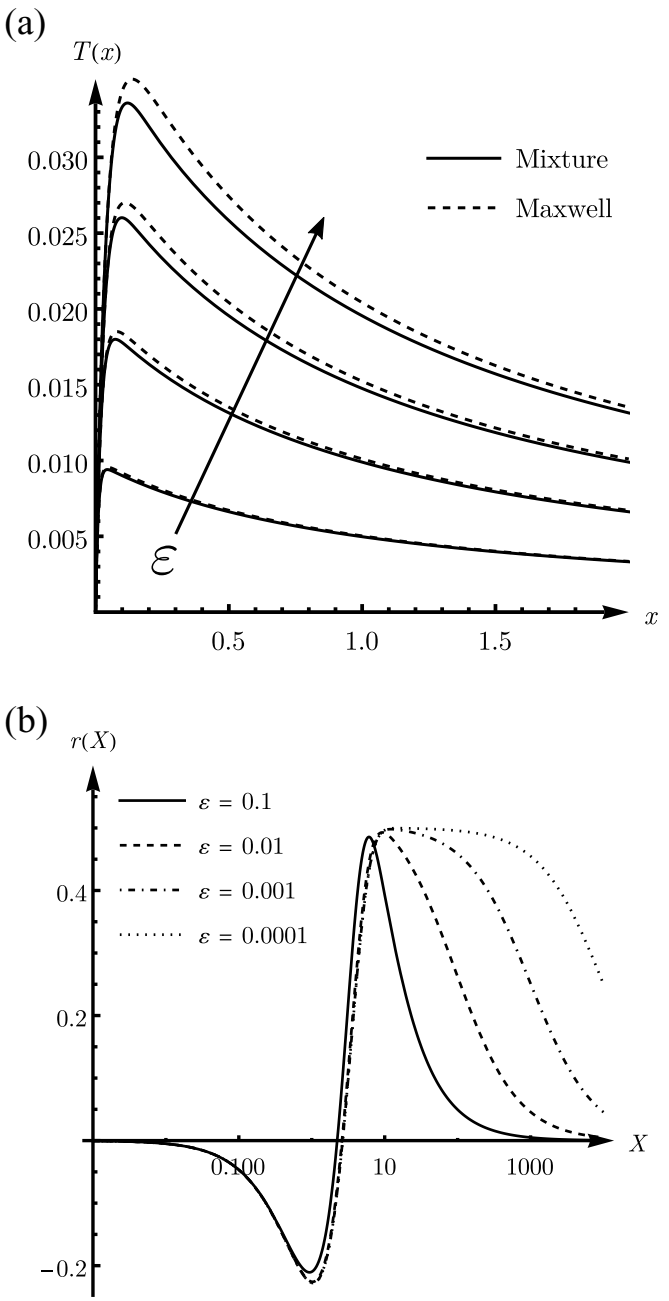

FIG. 6. (a) Tension-strain curve for the Maxwell model (dashed line) and the mixture models (solid line), for $\varepsilon = 0.01, 0.02, 0.03,$ and 0.04 and $q = 2$. (b) Logarithmic plot of the remainder $r(X)$, defined in Eq. (C15) vs $X = \varepsilon x$ for various values of ε and $q = 2$. We verify that $r(X) = \mathcal{O}(1)$ as $\varepsilon \to 0$.

Clearly, $\delta(x)$ is biggest for $x = \mathcal{O}(\varepsilon)$, and therefore, using $X := x/\varepsilon = \mathcal{O}(1)$, we have

$$\delta(X) \approx -\frac{\varepsilon X(X^2/2q - X - 1)}{e^X - 1} = \mathcal{O}(\varepsilon), \tag{C14}$$

namely, $T(x) = \widetilde{T}(x)(1 + \mathcal{O}(\varepsilon))$, which proves that to first order, the tension is given by the Maxwell model; see Fig. 6(a). We can also verify numerically that

$$r(x) = \frac{1}{\varepsilon}\left(1 - \frac{T(x)}{\widetilde{T}(x)}\right) \tag{C15}$$

is indeed $\mathcal{O}(1)$; see Fig. 6(b).

APPENDIX D: REINTRODUCTION OF CROSS LINKS

Next, we develop a numerical method to solve the integro-differential problem given by Eq. (9). From $S dx = k_{\text{on}} \widetilde{N} dt$ and $x = \xi t$, we obtain $\widetilde{N} = S\xi/k_{\text{on}} = S\nu/K$. Thus the governing equation for $\widetilde{N}$ can be recast so that it only involves S, as

$$\frac{dS}{dx} + \frac{S(x)}{\nu}\left(K + \frac{I_0}{k_{\text{off}}}\right) = \frac{I_0 N_0}{\nu^2 k_{\text{off}}}(1 + x) + \frac{\beta K}{\nu^2} R(x), \tag{D1}$$

where $R(x)$ is defined in Eq. (10). In the case where no new proteins are introduced ($I_0 = 0$), by virtue of the balance of mass, S is bounded and converges to $S_\infty \geqslant 0$, which can be determined by setting dS/dx to zero in Eq. (D1):

$$S_\infty = \lim_{x\to\infty} \frac{\beta}{\nu} \int_0^x S(x') \exp\left(\frac{1}{q}\frac{x - x'}{1 + x'}\right) \mathcal{G}(x, x')\, dx'. \tag{D2}$$

Using integration by part as in Appendix C 1, we also have

$$\lim_{x\to\infty} \int_0^x S(x') \exp\left(\frac{1}{q}\frac{x - x'}{1 + x'}\right) \mathcal{G}(x, x')\, dx' = \nu S_\infty. \tag{D3}$$

Thus, unsurprisingly, $S_\infty = 0$ if $\beta < 1$, as the probability of a protein being recycled n times is $\beta^n \to 0$. Conversely, if $\beta = 1$, proteins are endlessly disconnected and reintroduced, and the number of cross links stabilizes at $N_\infty = S_\infty \nu = N_0 K/(K + 1)$.

The general time-dependent problem in Eq. (D1) is solved numerically by discretizing the domain as a sequence $x_i = (i - 1)h$, $\forall i \in [1, n]$, with h a constant step size and n the desired number of evaluation points. We discretize Eq. (D1) using the backward Euler scheme,

$$\frac{S_i - S_{i-1}}{h} + \alpha_1 S_i = \alpha_2(1 + (i - 1)h) + \alpha_3 R_i, \tag{D4}$$

with S_i and R_i the estimated values of $S(x_i)$ and $R(x_i)$, respectively; and where

$$\alpha_1 = \frac{1}{\nu}\left(K + \frac{I_0}{k_{\text{off}}}\right), \quad \alpha_2 = \frac{I_0 N_0}{\nu^2 k_{\text{off}}}, \quad \alpha_3 = \frac{K\beta}{\nu^2} \tag{D5}$$

are dimensionless parameters. The integral part R_i is computed using the trapezoidal method with step size h:

$$\begin{aligned} R_i &= C_{i,1} + \frac{h}{2}\sum_{j=1}^{i-1} (C_{i,j+1} S_{j+1} + C_{i,j} S_j) \\ &= C_{i,1} + \frac{h}{2}(C_{i,1} S_1 + C_{i,i} S_i) + h\sum_{j=2}^{i-1} C_{i,j} S_j, \end{aligned} \tag{D6}$$

where

$$C_{i,j} = \mathcal{G}(x_i, x_j) \exp\left(\frac{1}{q}\frac{x_i - x_j}{1 + x_j}\right) \tag{D7}$$

are precomputed coefficients defined for $0 \leqslant j \leqslant i \leqslant n$.

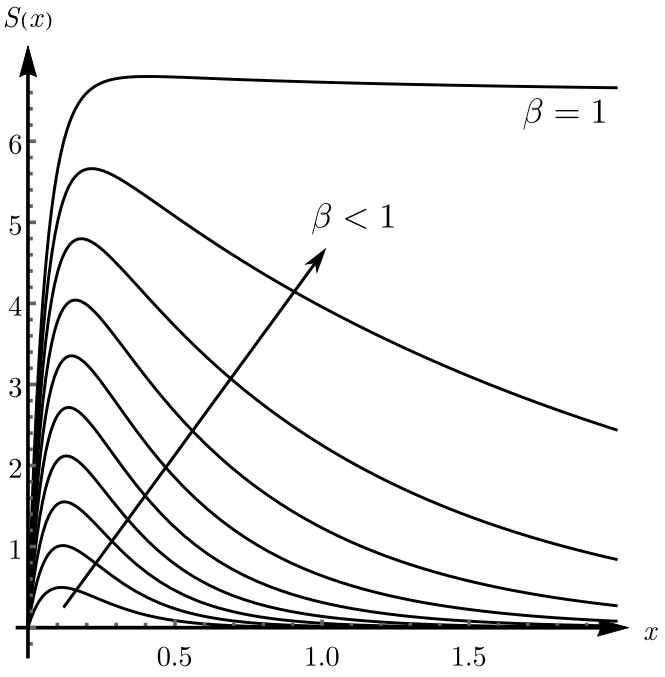

FIG. 7. Reintroduction of disconnected cross links. Binding rate $S(x)$ vs x for various values of β. Here we consider the case where no new proteins are introduced ($I_0 = 0$).

Finally, combining Eqs. (D6) and (D4), we obtain the iterative integration algorithm,

$$S_i = \mathbb{A}_i + \sum_{k=1}^{i-1} \mathbb{B}_{i,k} S_k, \tag{D8}$$

where, for all $i \in [1, n]$,

$$\mathbb{A}_i = \frac{h\alpha_3 C_{i,1} + h\alpha_2(1 + (i-1)h)}{1 + h\alpha_1 - h^2\alpha_3 C_{i,i}/2}, \tag{D9}$$

and, for all $k \in [1, i-1]$,

$$\mathbb{B}_{i,k} = \begin{cases} \frac{h^2\alpha_3 C_{i,1}/2}{1+h\alpha_1-h^2\alpha_3 C_{i,i}/2} & \text{if } k = 1, \\ \frac{1+h^2\alpha_3 C_{i,i-1}}{1+h\alpha_1-h^2\alpha_3 C_{i,i}/2} & \text{if } k = i-1, \\ \frac{h^2\alpha_3 C_{i,k}}{1+h\alpha_1-h^2\alpha_3 C_{i,i}/2} & \text{otherwise.} \end{cases} \tag{D10}$$

Figure 7 shows computed profiles for $S(x)$, for various values of $\beta \in [0, 1]$, and in the case where no new proteins are introduced ($I_0 = 0$).

APPENDIX E: COMPARISON WITH DISCRETE MODEL

In this section, we adapt our parameters to the particular setting developed in [32]. In the cited work, the cross links are modeled as Hookean rods with Young's modulus 10 MPa and cross-sectional area 1 nm^2. The cross-link lengths can vary depending on the relative positions of the two anchoring points in the simulation; here, we select the average value 150 nm as the reference cross-link length. We deduce the spring constant 0.03 pN nm^{-1}. Note, however, that in the computational model, cross links are attached with an average angle $\beta \approx 45^\circ$ with respect to the microtubule axis. Thus the equivalent longitudinal spring constant is actually $\kappa = \kappa^* \cos^2\beta = \kappa^*/2$. All other relevant parameters are identical to those used in [32].

[1] M. A. Patestas and L. P. Gartner, *A Textbook of Neuroanatomy*, 2nd ed. (Wiley, New York, 2016).

[2] G. F. Striedter, *Neurobiology: A Functional Approach*, 1st ed. (Oxford University Press, Oxford, 2016).

[3] K. Franze, Integrating chemistry and mechanics: The forces driving axon growth, Annu. Rev. Cell Dev. Biol. **36**, 61 (2020).

[4] L. E. McCormick and S. L. Gupton, Mechanistic advances in axon pathfinding, Curr. Opin. Cell Biol. **63**, 11 (2020).

[5] D. H. Smith, Stretch growth of integrated axon tracts: Extremes and exploitations, Prog. Neurobiol. **89**, 231 (2009).

[6] B. J. Pfister, A. Iwata, D. F. Meaney, and D. H. Smith, Extreme stretch growth of integrated axons, J. Neurosci. **24**, 7978 (2004).

[7] M. A. Holland, K. E. Miller, and E. Kuhl, Emerging brain morphologies from axonal elongation, Ann. Biomed. Eng. **43**, 1640 (2015).

[8] K. E. Miller and D. M. Suter, An integrated cytoskeletal model of neurite outgrowth, Front. Cell. Neurosci. **12**, 447 (2018).

[9] P. K. Purohit and D. H. Smith, A model for stretch growth of neurons, J. Biomech. **49**, 3934 (2016).

[10] M. O'Toole and K. E. Miller, The role of stretching in slow axonal transport, Biophys. J. **100**, 351 (2011).

[11] D. H. Smith and D. F. Meaney, Axonal damage in traumatic brain injury, The Neuroscientist **6**, 483 (2000).

[12] A. Goriely, S. Budday, and E. Kuhl, Neuromechanics: From neurons to brain, in *Advances in Applied Mechanics*, Vol. 48, edited by S. P. Bordas and D. S. Balint (Academic Press, Cambridge, MA, 2015), Chap. 2, pp. 79–139.

[13] R. de Rooij and E. Kuhl, Physical biology of axonal damage, Front. Cell. Neurosci. **12**, 144 (2018).

[14] R. M. Wright, A. Post, B. Hoshizaki, and K. T. Ramesh, A multiscale computational approach to estimating axonal damage under inertial loading of the head, J. Neurotrauma **30**, 102 (2013).

[15] H. van den Bedem and E. Kuhl, Tau-ism: The yin and yang of microtubule sliding, detachment, and rupture, Biophys. J. **109**, 2215 (2015).

[16] M. D. Tang-Schomer, A. R. Patel, P. W. Baas, and D. H. Smith, Mechanical breaking of microtubules in axons during dynamic stretch injury underlies delayed elasticity, microtubule disassembly, and axon degeneration, FASEB J. **24**, 1401 (2010).

[17] H. Oliveri, K. Franze, and A. Goriely, Theory for Durotactic Axon Guidance, Phys. Rev. Lett. **126**, 118101 (2021).

[18] T. J. Dennerll, P. Lamoureux, R. E. Buxbaum, and S. R. Heidemann, The cytomechanics of axonal elongation and retraction, J. Cell Biol. **109**, 3073 (1989).

[19] R. Bernal, P. A. Pullarkat, and F. Melo, Mechanical properties of axons, Phys. Rev. Lett. **99**, 018301 (2007).

[20] G. H. Li and C. D. Qin, A model for neurite growth and neuronal morphogenesis, Math. Biosci. **132**, 97 (1996).

[21] M. O'Toole, P. Lamoureux, and K. E. Miller, A physical model of axonal elongation: Force, viscosity, and adhesions govern the mode of outgrowth, Biophys. J. **94**, 2610 (2008).

[22] M. O'Toole, P. Lamoureux, and K. E. Miller, Measurement of subcellular force generation in neurons, Biophys. J. **108**, 1027 (2015).

[23] J. Lin, X. Li, J. Yin, and J. Qian, Effect of cyclic stretch on neuron reorientation and axon outgrowth, Front. Bioeng. Biotechnol. **8**, 1429 (2020).

[24] A. Goriely, *The Mathematics and Mechanics of Biological Growth*, 1st ed., edited by S. S. Antman, L. Greengard, and P. J. Holmes, Interdisciplinary Applied Mathematics, Vol. 45 (Springer-Verlag, New York, 2017).

[25] L. M. Wang and E. Kuhl, Viscoelasticity of the axon limits stretch-mediated growth, Comput. Mech. **65**, 587 (2020).

[26] H. Oliveri and A. Goriely, Mathematical models of neuronal growth, Biomech. Model. Mechanobiol. **21**, 89 (2022).

[27] A. Shamloo, F. Manuchehrfar, and H. Rafii-Tabar, A viscoelastic model for axonal microtubule rupture, J. Biomech. **48**, 1241 (2015).

[28] S. J. Peter and M. R. Mofrad, Computational modeling of axonal microtubule bundles under tension, Biophys. J. **102**, 749 (2012).

[29] M. A. H. Jakobs, K. Franze, and A. Zemel, Force generation by molecular-motor-powered microtubule bundles; implications for neuronal polarization and growth, Front. Cell. Neurosci. **9**, 441 (2015).

[30] M. A. H. Jakobs, K. Franze, and A. Zemel, Mechanical regulation of neurite polarization and growth: A computational study, Biophys. J. **118**, 1914 (2020).

[31] R. de Rooij, K. E. Miller, and E. Kuhl, Modeling molecular mechanisms in the axon, Comput. Mech. **59**, 523 (2017).

[32] R. de Rooij and E. Kuhl, Microtubule polymerization and cross-link dynamics explain axonal stiffness and damage, Biophys. J. **114**, 201 (2018).

[33] R. de Rooij, E. Kuhl, and K. E. Miller, Modeling the axon as an active partner with the growth cone in axonal elongation, Biophys. J. **115**, 1783 (2018).

[34] A. Montanino and S. Kleiven, Utilizing a structural mechanics approach to assess the primary effects of injury loads onto the axon and its components, Front. Neurol. **9**, 643 (2018).

[35] A. Montanino, M. Saeedimasine, A. Villa, and S. Kleiven, Localized axolemma deformations suggest mechanoporation as axonal injury trigger, Front. Neurol. **11**, 1 (2020).

[36] H. Ahmadzadeh, D. H. Smith, and V. B. Shenoy, Viscoelasticity of tau proteins leads to strain rate-dependent breaking of microtubules during axonal stretch injury: Predictions from a mathematical model, Biophys. J. **106**, 1123 (2014).

[37] H. Ahmadzadeh, D. H. Smith, and V. B. Shenoy, Mechanical effects of dynamic binding between tau proteins on microtubules during axonal injury, Biophys. J. **109**, 2328 (2015).

[38] C. Lazarus, M. Soheilypour, and M. R. Mofrad, Torsional behavior of axonal microtubule bundles, Biophys. J. **109**, 231 (2015).

[39] N. Liu, P. Chavoshnejad, S. Li, M. J. Razavi, T. Liu, R. Pidaparti, and X. Wang, Geometrical nonlinear elasticity of axon under tension: A coarse-grained computational study, Biophys. J. **120**, 3697 (2021).

[40] R. M. Christensen, *Theory of Viscoelasticity: An Introduction*, 2nd ed. (Academic Press, Cambridge, MA, 1982).

[41] N. Hirokawa, Y. Shiomura, and S. Okabe, Tau proteins: the molecular structure and mode of binding on microtubules., J. Cell Biol. **107**, 1449 (1988).

[42] F. Meng, R. H. Pritchard, and E. M. Terentjev, Stress relaxation, dynamics, and plasticity of transient polymer networks, Macromolecules **49**, 2843 (2016).

[43] G. I. Bell, Models for the specific adhesion of cells to cells, Science **200**, 618 (1978).

[44] J. A. Tuszyński, T. Luchko, S. Portet, and J. M. Dixon, Anisotropic elastic properties of microtubules, Eur. Phys. J. E **17**, 29 (2005).

[45] R. Mallik, B. C. Carter, S. A. Lex, S. J. King, and S. P. Gross, Cytoplasmic dynein functions as a gear in response to load, Nature (London) **427**, 649 (2004).

[46] F. Gittes, B. Mickey, J. Nettleton, and J. Howard, Flexural rigidity of microtubules and actin filaments measured from thermal fluctuations in shape, J. Cell Biol. **120**, 923 (1993).

[47] F. Pampaloni, G. Lattanzi, A. Jonáš, T. Surrey, E. Frey, and E.-L. Florin, Thermal fluctuations of grafted microtubules provide evidence of a length-dependent persistence length, Proc. Natl. Acad. Sci. USA **103**, 10248 (2006).

[48] M. Igaev, D. Janning, F. Sündermann, B. Niewidok, R. Brandt, and W. Junge, A refined reaction-diffusion model of tau-microtubule dynamics and its application in FDAP analysis, Biophys. J. **107**, 2567 (2014).

[49] P. Recho, A. Jérusalem, and A. Goriely, Growth, collapse, and stalling in a mechanical model for neurite motility, Phys. Rev. E **93**, 032410 (2016).

[50] A. Datar, J. Ameeramja, A. Bhat, R. Srivastava, A. Mishra, R. Bernal, J. Prost, A. Callan-Jones, and P. A. Pullarkat, The roles of microtubules and membrane tension in axonal beading, retraction, and atrophy, Biophys. J. **117**, 880 (2019).

[51] M. O'Toole, R. Latham, R. M. Baqri, and K. E. Miller, Modeling mitochondrial dynamics during in vivo axonal elongation, J. Theor. Biol. **255**, 369 (2008).